REVIEW PAPER

The metal magnetic memory method application for online monitoring of damage development in steel pipes and welded joints specimens

Anatoly Dubov · Sergey Kolokolnikov

Abstract The magnetic memory of metal (MMM) is an after-effect, which occurs in the form of metal residual magnetization in components and welded joints formed in the course of their fabrication and cooling in the weak magnetic field of the earth and in the form of irreversible change of components' magnetization in zones of stress concentration and damages under working loads (ISO 24497–1:2007(E)). The results of experimental investigation by the metal magnetic memory of steel specimens in the process of their static and cyclic loading are presented. Investigation using the MMM method was carried out online in the process of cyclic loading in the synchronous manner with load frequency. Specific features of self-magnetic field's (SMLF) intensity variation at maximum load during tensile cyclic load were revealed. The obtained results of specimens investigation experimentally confirmed the earlier drawn conclusion about the possibility of the MMM method and corresponding inspection instruments application for quick testing of mechanical properties and cyclic strength parameters at the physical level. Comparison of $\sigma-\varepsilon$ deformation curves and $\sigma-\Delta H_x$, $\Delta H_x-\varepsilon$ magnetograms, obtained in the static loading mode, of $\sigma-\varepsilon$ cyclic loading profiles and corresponding magnetograms confirms once more the earlier established correlation of magneto-mechanical parameters conditioned by the "magnetodislocation hysteresis". Fatigue curves, plotted by variation of the self-magnetic field of the specimens in the process of cyclic loading, experimentally confirm the possibility of equipment life assessment by parameters of the metal's magnetic memory. Magnetograms, recorded online in the process of cyclic loading of specimens, allow claiming the possibility of the MMM method and the Tester of Stress Concentration type instruments application for technical state monitoring during operation of equipment under load conditions.

1 Introduction

Physical bases of the metal magnetic memory (MMM) method were presented in the papers [1, 2]. Paper [2] presents general inspection techniques and operating principle of MMM inspection devices. Vocabulary and general requirements to the inspection, including welded joints testing, were presented in the ISO standards [3–5].

Some results of investigation of mechanical and physical properties of steel specimens using the metal magnetic memory method were presented in papers [6–8]. The aforementioned investigations were carried out basically under the conditions of static tensile loading. The paper [2] presents some fragments of investigations of steel specimens under the conditions of cyclic tensile loading using the MMM method.

The need to check experimentally the correlation of diagnostic parameters with strain prompted carrying out of static and cyclic load testing of steel specimens by the MMM method. MMM method application for online monitoring of damage developing is also conditioned by the existing drawbacks in practical realization of cyclic strength testing of specimens.

These include, first of all, the difficulty of ensuring the continuous recording of the strain diagram synchronously with

A. Dubov · S. Kolokolnikov (✉)
Energodiagnostika Co. Ltd, Moscow, Russia
e-mail: mail@energodiagnostika.ru

the amplitude and frequency of the load during the entire period of the cyclic load application right up to failure of the specimen. For recording of strain cycling diagrams in the course of loading, as a rule, lower frequencies are selected in order to ensure the recording accuracy of load parameters.

Secondly, there are no available physical methods of experimental investigations, which would allow the real-time tracing, synchronously with the load frequency, of physical processes of resistance to strain, occurring in the metal of specimens, in the course of cyclic loading.

During the last years, attempts have been made to use the acoustic emission (AE) method for this purpose. However, impossibility to install the AE sensors directly in the area of the assumed failure of the specimen and presence of the extraneous noise generated by operation of the testing machine complicate the AE investigations during such tests.

The first attempts to use the MMM and the appropriate inspection instruments for this purpose, presented in the paper [2], showed good results. MMM method inspection instruments use small-size sensors (e.g., flux gate transducers) for measurement of the self-magnetic leakage field (SMLF) intensity H_L. Fluxgate transducers are used for inspection tools of the MMM method for measuring weak self-magnetic leakage fields in range of ±2,000 A/m. Flux-gate transducers are usually equipped with two coils: excitation coil and pick-off coil. These coils usually have a core (wireshaped, toroid, oval, etc.). The basic property of flux-gate sensor is that the sensor core is periodically saturated by the excitation current and that its output is on the second harmonic (or higher even harmonic) of the excitation frequency. One, two, or three orthogonal axis fluxgate sensor can be applied for testing by using the MMM method for measurement of SMLF intensity of up to three rectangular components in three dimensions, respectively.

The small-sized sensors allow to install them directly near the location of the assumed failure (with the accuracy of up to 1 mm). At the same time, in contrast to the AE sensors, the direct contact of the sensor with the surface of the specimen is not required. Besides, the use of two- and three-component sensors allows, due to the magnetomechanical effect, tracing the variation of the strain amplitude in three directions: in the longitudinal (coaxially with the direction of the internal load—H_L^X), transverse (perpendicular to the applied load—H_L^Z) and radial direction (perpendicular to the test surface—H_L^Y). At the same time, the specialized Tester of Stress Concentration (TSC) instruments,[1] equipped with a screen and a memory unit of 32 MB and higher, when operated in the "timer" mode

(measurement of SMLF intensity of each components, data logging and graph plotting can be performed with high frequency up to 3 kHz) ensure continuous observation of the cyclic loading process of the specimen as well as online recording of measurement results of magnetic parameters synchronously with the applied cyclic load in a wide range of frequencies variation (from 1 to 300 Hz).

2 Background

Figure 1 shows the shape and dimensions of the steel specimens used for cyclic tensile load tests. The cross-section restriction was made in the middle part of the specimens in
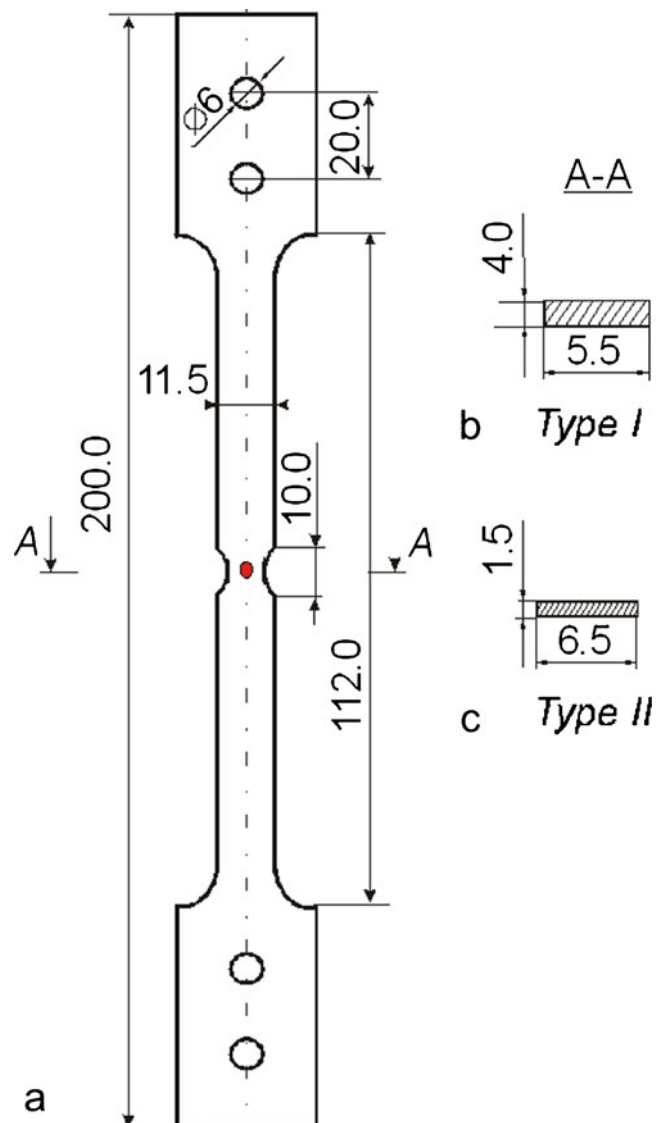

Fig. 1 The shape and dimensions of specimens (**a**) for cyclic tensile load tests: *A-A* cross-section of the specimens of the type I (**b**) and of the type II (**c**). *SCZ* the stress concentration zone, the inspection area

---

[1] In Russia, for testing by MMM method special instruments—TSC (manufacturer Energodiagnostika Co. Ltd.) were certified by Federal Agency on Technical Regulating and Metrology (the National Standards Body) of the Russian Federation.

Table 1 Chemical composition (percent) of steel 10 CrSND (GOST 19282)

C	Si	Mn	Ni	S	P	Cr	N	Cu	As
0.12	0.80–1.1	0.50–0.80	0.50–0.80	0.04	0.035	0.60–0.90	0.008	0.40–0.60	0.08

order to determine the location of the assumed failure and of the maximum deformation of the specimen and, respectively, in order to determine the location of the TSC instrument sensor installation. The Ø6mm holes on the holders of the specimen were made to fit the bolted joints with holders of the testing machine.

Two types of specimens were tested:

– type I, the material was the structural steel 10CrSND with the yield strength σ_y=450 MPa, ultimate strength σ_{ult}=570 MPa and the area of the cross-section F=5,5× 4=22 mm^2. Chemical composition of steel 10 CrSND is presented in the Table 1
– type II, the material was low-carbon normal quality steel 3sp (corresponding steel grade ASTM A 283 grade C) with the yield strength σ_y=250 MPa, ultimate strength σ_{ult}=350 MPa and the area of the cross-section F=6,5×1,5=9,75 mm^2. Chemical composition of Steel 3 is presented in the Table 2.

Four specimens of the type I and five specimens of the type II were tested in total.

Figure 2 shows the scheme of measurement of the normal and the tangential (in the direction of the applied load P) components of the self-magnetic field of the specimen placed in the tensile testing machine. The specimen 2, which has a special groove 3 for localization of the inspection area, was fixed in the attachment unit 1 of the tensile-testing machine using two bolted joints. The two-component sensor 4, allowing to measure the tangential H_L^X and the normal H_L^Y components of the magnetic field near the surface of the specimen (at the distance of 0.5÷1.0 mm), is installed in the holder 6 and fixed in it rigidly in one position. The electronic unit 5—the analog digital transducer—was connected to the recording TSC instrument.

It should be specially noted that the gap between the recording sensors and the specimen's surface allows, along with precise SMLF intensity measurement, to ensure mechanical stability of inspection plant, thus removing undesirable disturbances and damages due to vibration loads occurring inevitably during contact inspection.

Testing of specimens under static and cyclic loads according to the measurement scheme, presented in Fig. 2, was carried out at the A.A. Blagonravov Institute of Engineering Science of Russian Academy of Sciences (Moscow) using the testing machine "Material Test System (MTS) 311.21".

Let us further consider some results of steel specimens investigation during application of the static and cyclic tensile load in the range from 1 to 10 Hz.

3 Investigation of steel specimens SMLF under applied tensile stress

One specimen of each type was preliminarily subject to static tensile testing in order to determine the actual values of σ_y and σ_t. At the same time, simultaneous recording (in the mode of the real-time application of the tensile load) of the strain diagram by the recording device of the testing machine and of variation of the normal (H_L^Y) and the tangential (H_L^X) components of the magnetic field in the SCZ of the specimen was performed.

Figure 3 presents comparison of the strain diagram σ–ε and the variation diagram of the tangential component intensity increase H_L^X of the SMLF depending on tensile stresses for the specimen of the type I.

Figure 4 shows variation of the tangential component intensity increase H_L^X of the SMLF depending on strain ε, obtained based on the results of measurements in SCZ (the neck zone) for the specimens of the type I.

Figure 5 presents comparison of the strain diagram σ–ε and the variation diagram of the tangential component intensity increase H_L^X of the SMLF depending on tensile stresses for the specimen of the type II.

Figure 6 shows variation of the tangential component intensity increase H_L^X of the SMLF depending on strain ε, obtained based on the results of measurements in SCZ (the neck zone) for the specimens of the type II.

Figures 3 and 5 show good correlation between the obtained diagrams, which confirms the proportional dependence of variation of the self-magnetic field H_L^X of the specimen on the tensile strain at the physical level.
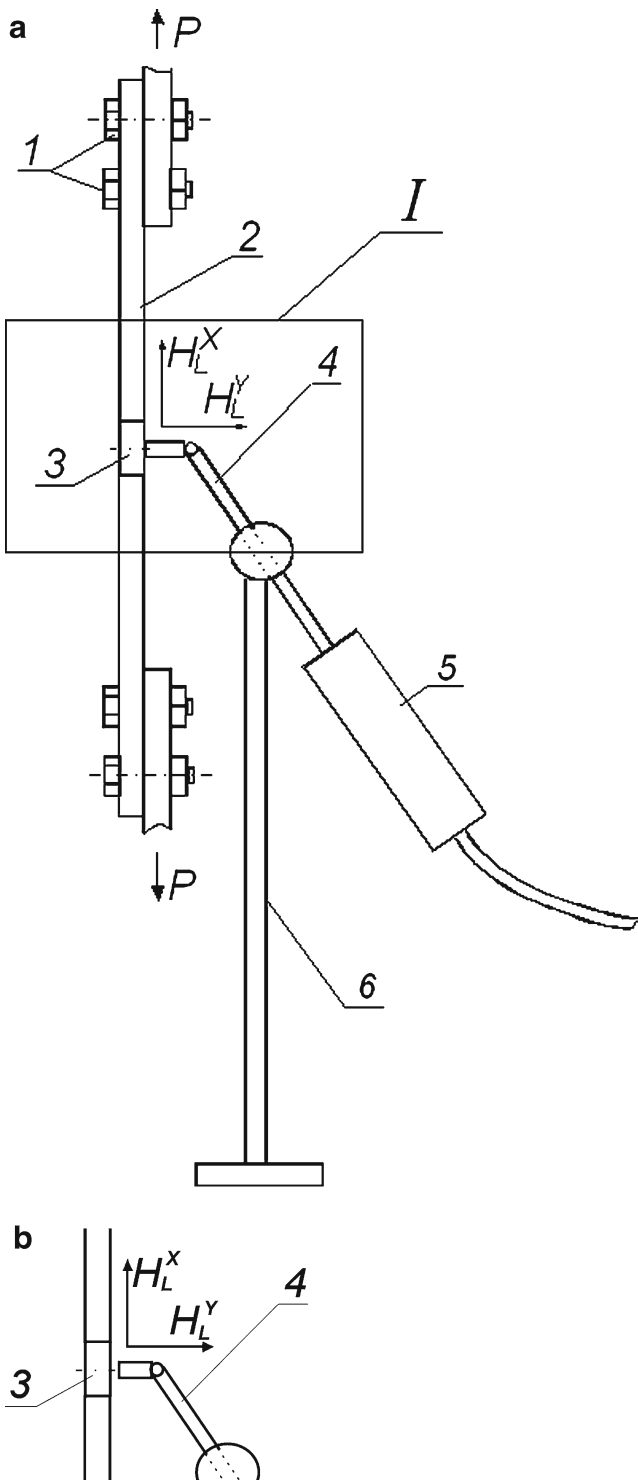
Table 2 Chemical composition (percent) of steel 3sp (GOST 380)

C	Si	Mn	Ni	S	P	Cr	N	Cu	As
0.14–0.22	0.15–0.3	0.4–0.65	0.3	0.05	0.04	0.3	0.008	0.3	0.08

a

b

Fig. 2 The scheme of measurement of the normal (H_L^Y) and tangential (H_L^x) components of the self-magnetic field of the specimen: *1* point of the specimen attachment in the tensile-testing machine, *2* the specimen, *3* the groove for localization of the inspection area, *4* the sensor, *5* the electronic unit, *6* the holder for attachment of the sensor, *P* tensile load

Figures 4 and 6 show that the dependence $H_L^x = f(e)$ has the nature which is close in with the linear one. Some differences can be appeared due to uncertainties of measurement procedure.

4 Investigation of steel specimens SMLF under applied cyclic load

Then three specimens (#2, #3, #4) of the type I and four specimens (#2, #3, #4, #5) of the type II were tested for cyclic tensile load at different frequencies. Specimens of the type I were tested in the range of the tensile load from $P_{\min}=$ 100 kg to $P_{\max}=950$ kg or $(0.2 \div 0.95)\sigma_y$.

Specimens of the type II were tested in the range of the tensile load from $P_{\min}=50$ kg to $P_{\max}=250$ kg or $(0.2 \div 1.0)\sigma_y$. Figures 7 and 8 present time dependences of the normal H_L^Y and the tangential H_L^X components of the magnetic field on the cyclic load, obtained during testing, respectively, for the specimen #3 of the type I (at the frequency of 2 Hz) and for the specimen #4 of the type I (at the frequency of 10 Hz).

The general rules, which can be marked out based on the analysis of the magnetograms, presented in Figs. 7 and 8, are the following:
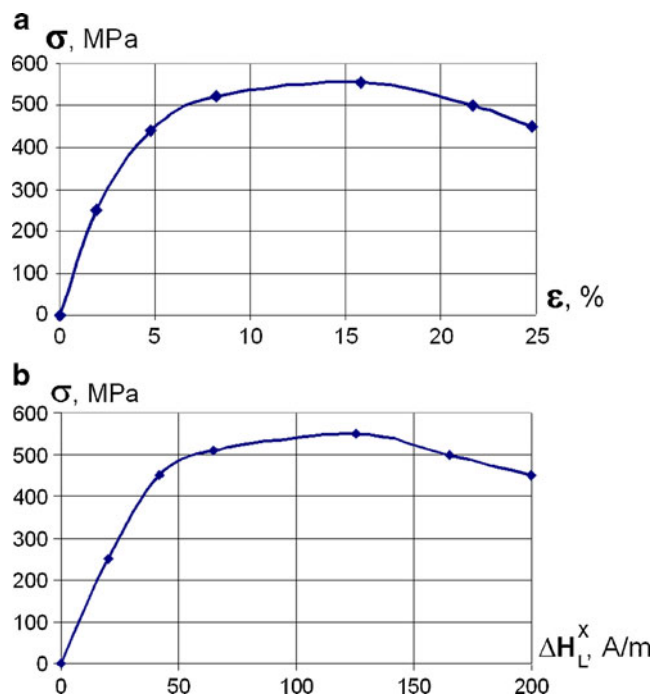
a

b

Fig. 3 Comparison of the strain diagram σ–ε (**a**) and the variation diagram of the tangential component intensity increase H_L^X of the SMLF (**b**) depending on tensile stresses for the specimen of the type I
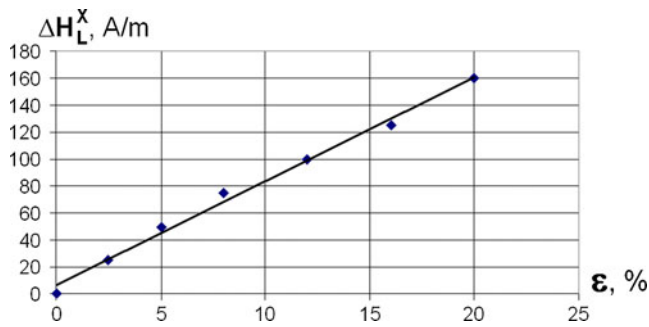
Fig. 4 Variation of the tangential component intensity increase H_L^x of the SMLF depending on strain, obtained at tension of the specimen of the type I
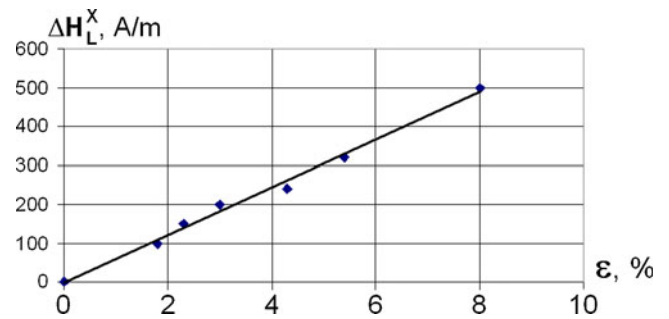

Fig. 6 Variation of the tangential component intensity increase H_L^x of the SMLF depending on strain, obtained at tension of the specimen of the type II

- coincidence by the frequency of the applied load and of the amplitude variation of the components H_L^Y and H_L^X of the field
- minor amplitude variation of the value of the field components H_L^Y and H_L^X from the amplitude of the applied load at all stages of load cycles N right up to failure of the specimens
- abrupt change of the magnetic field normal H_L^Y and tangential H_L^X components were observed at the moment of the crack opening and subsequent rupture of the specimen
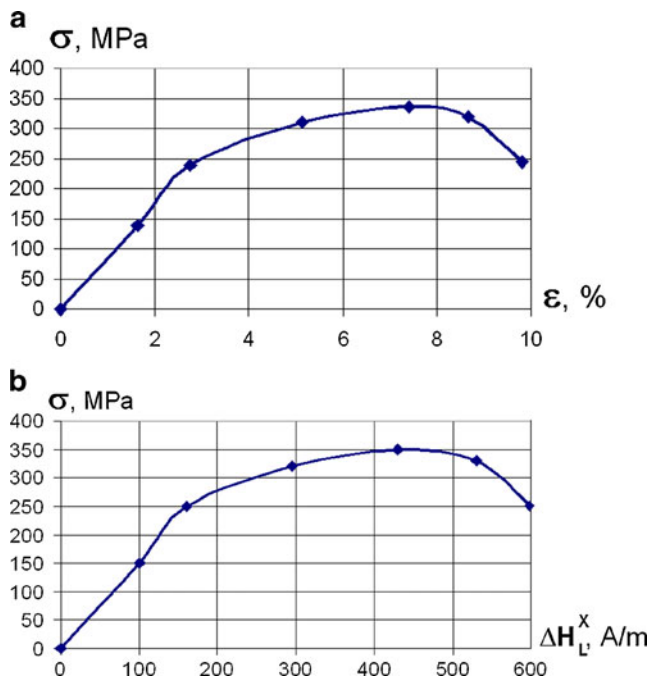

Fig. 5 Comparison of the strain diagram σ–ε (**a**) and the variation diagram of the tangential component intensity increase H_L^X of the SMLF (**b**) depending on tensile stresses for the specimen of the type II
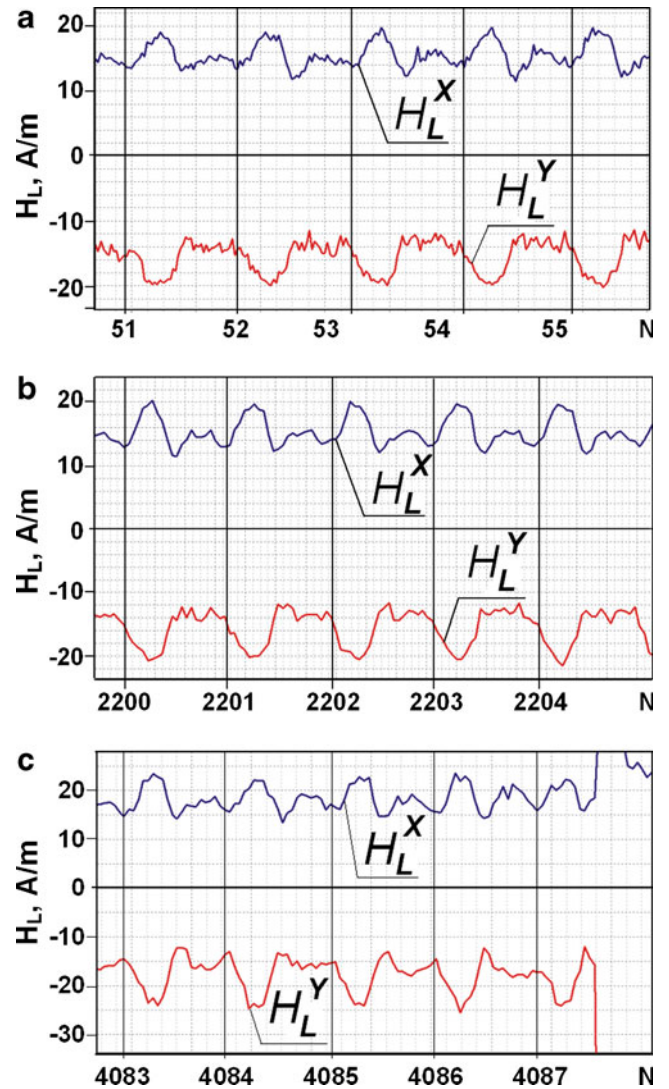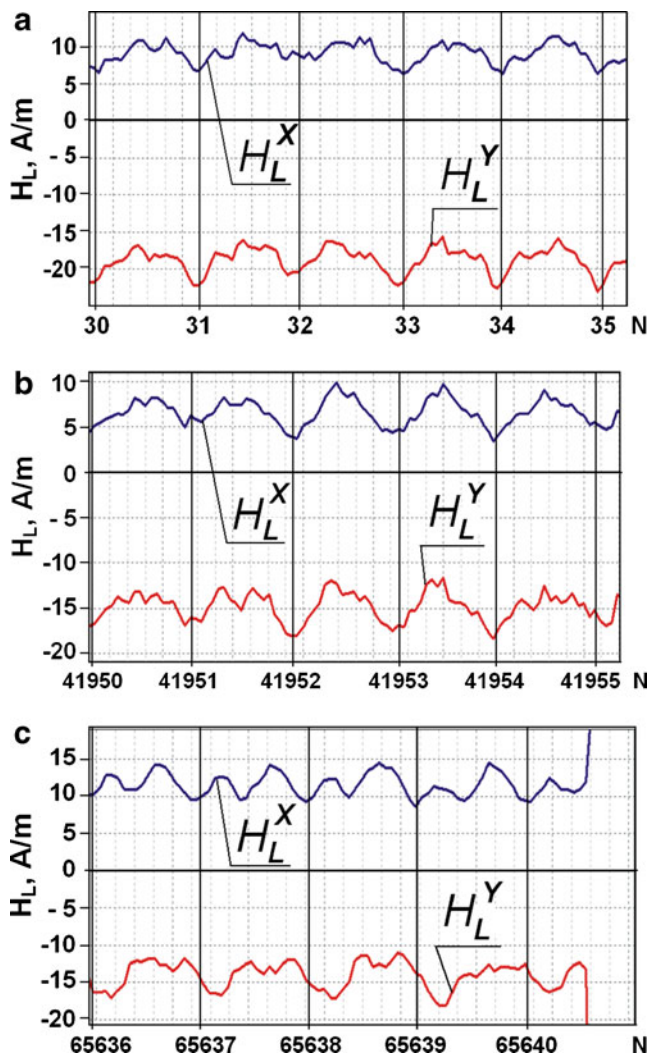

Fig. 7 Time dependence of the normal H_L^Y and the tangential H_L^X components of the magnetic field H_L on the cyclic tensile load at the frequency of 2 Hz for the specimen #3 of the type I: **a** the initial stage, **b** the established mode, **c** the final stage

Fig. 8 Time dependence of the normal H_L^Y and the tangential H_L^X components of the magnetic field H_L on the cyclic tensile load at the frequency of 10 Hz for the specimen #4 of the type I: **a** the initial stage, **b** the established mode, **c** the final stage

– the number of cycles before failure of the specimen increases significantly with increasing of the frequency of the applied load from 2 to 10 Hz

Figure 9 shows the time dependence of the tangential H_L^X component of the magnetic field on the cyclic tensile load, obtained during testing of the specimen #2 of the type II at different stages of cyclic straining right up to failure. Based on the presented in Fig. 9 magnetograms, the following specific features can be pointed out:

– notable increasing of the amplitude variation of the H_L^X component of the field with increasing of the number of load cycles N (at the initial stage the modular variation

is $|\Delta H_x| \approx 150$ A/m, in the established mode—$|\Delta H_x| \approx 200$ A/m and at the final stage—$|\Delta H_x| \approx 350$ A/m);

– the effect of abrupt decline and instantaneous growth of the field H_L^X was recorded at the maximum of the applied load P_{max} of each cycle. The aforementioned effect was not observed at the minimum of the cyclic load amplitude P_{min}. This effect was observed for both components of the field H_y and H_x, both for the specimens of the type II and for the specimens of the type I (see Figs. 7 and 8)

– abrupt change of the magnetic field tangential H_L^X component was observed at the moment of the crack opening and subsequent rupture of the specimen

Figure 10 demonstrates typical abrupt variation of the SMLF intensity at the moment of the crack opening and subsequent rupture of the small-scale specimens. Usually, the SMLF value at the moment of crack opening and subsequent rupture exceeds average value up to two to five times.

It should be noted that the display of the effect of short-time decline and growth of the field components H_L^Y and H_L^X at the maximum of the cyclic tensile load increases gradually as the number of cycles grows and meets the maximum value by the amplitude directly before failure of the specimen. On both specimens of the type II (Steel 3) the variation amplitude of the field components H_L^Y and H_L^X is notably greater as compared to the specimens of the type I (Steel 10CrSND).

Figure 11 presents the diagram of cyclic straining σ–ε, recorded on the specimen #2 of the type II for cyclic tensile loading in the range of $(0.2 \div 1.0)\sigma_y$. In this diagram, the frequency of load application was reduced from 3 to 1 Hz and lower. The comparison of Figs. 11 and 9 demonstrates that the diagram σ–ε does not observe the effect of short-time growth and decline of resistance to straining at the maximum of the applied load.

However, the general pattern of the curve σ–ε (the width of the loop) at the load maximum corresponds to the magnetogram presented in Fig. 9. At the minimum of the cyclic load, the appearance of the diagram σ–ε practically corresponds to the magnetogram presented in Fig. 9.

Figures 12 and 13 present variation of the tangential component intensity increase H_L^X of the SMLF depending on the number of load cycles N, recorded during testing, respectively, of the specimen #4 of the type I and of the specimen #2 of the type II.

According to the rules established in the paper [1], the curves $H_L^X = f(N)$, presented in Figs. 12 and 13, qualitatively correspond to fatigue curves of the metal of the specimens.

These curves provide a unique opportunity to carry out the assessment of the process of fatigue time-dependent failure of the specimens depending on the number of cycles and the load frequency and amplitude. It should be noted

Fig. 9 Time dependence of the tangential H_L^X component of the magnetic field H_L on the cyclic tensile load at the frequency of 3 Hz for the specimen #2 of the type II: **a**, **b** the initial stage; **c** the established mode; **d** the final stage; *1* positions of the curve H_L^X, recorded at the moment of application of the maximum load P_{max}; *2* positions of the curve H_L^X, recorded at the moment of application of the minimum load P_{min}; *3* variation of the magnetic field tangential component H_L^X at the moment of the crack opening and subsequent rupture of the specimen
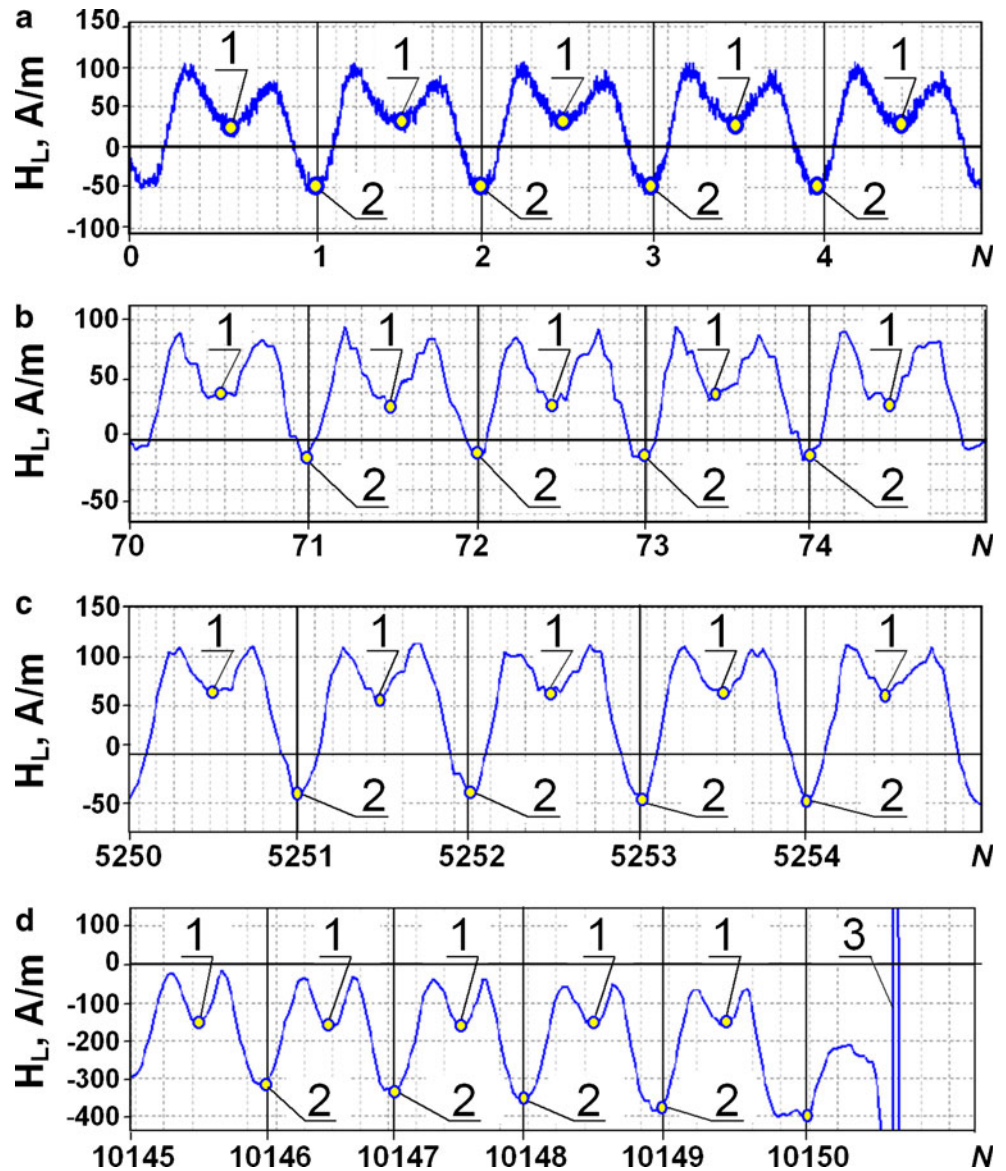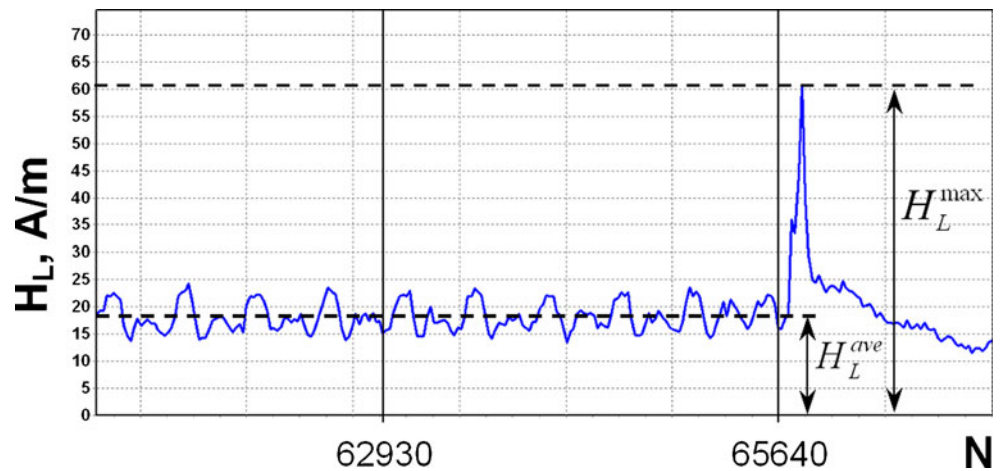
Fig. 10 Typical variation of the SMLF intensity at the moment of the crack opening and subsequent rupture of the specimen
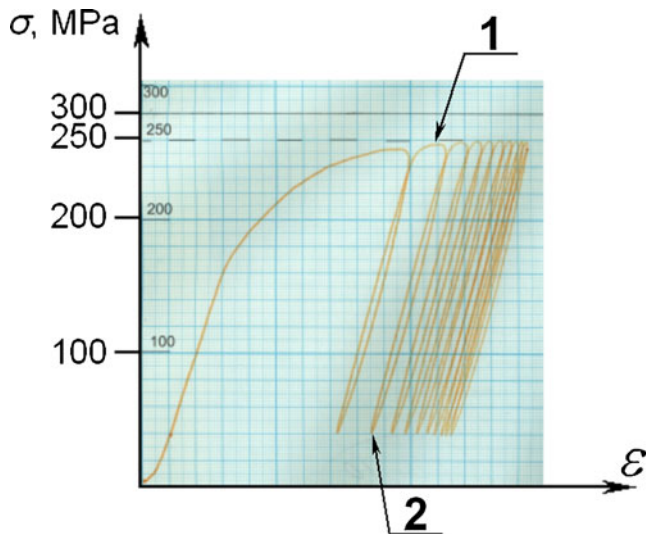
Fig. 11 The diagram of cyclic straining σ–ε, recorded on the specimen #2 of the type II: *1* positions on the diagram that corresponded to the maximum load P_{max}; *2* positions on the diagram that corresponded to the minimum load P_{min}

Fig. 13 Variation of the tangential component intensity increase H_L^X of the SMLF in the point A of the specimen #4 of the type II depending of the number of tensile load cycles $(0.2 \div 0.95)\sigma_y$ at the frequency of 3 Hz
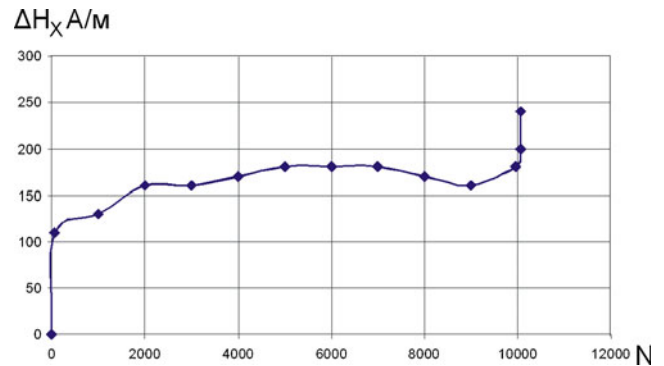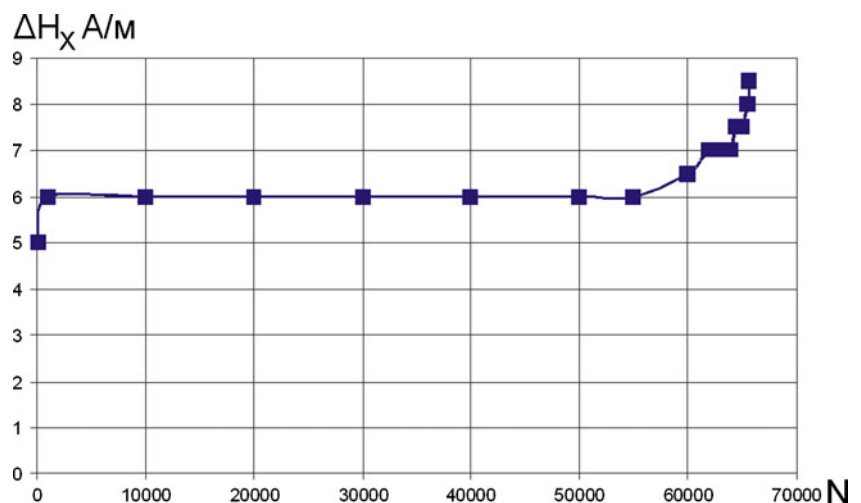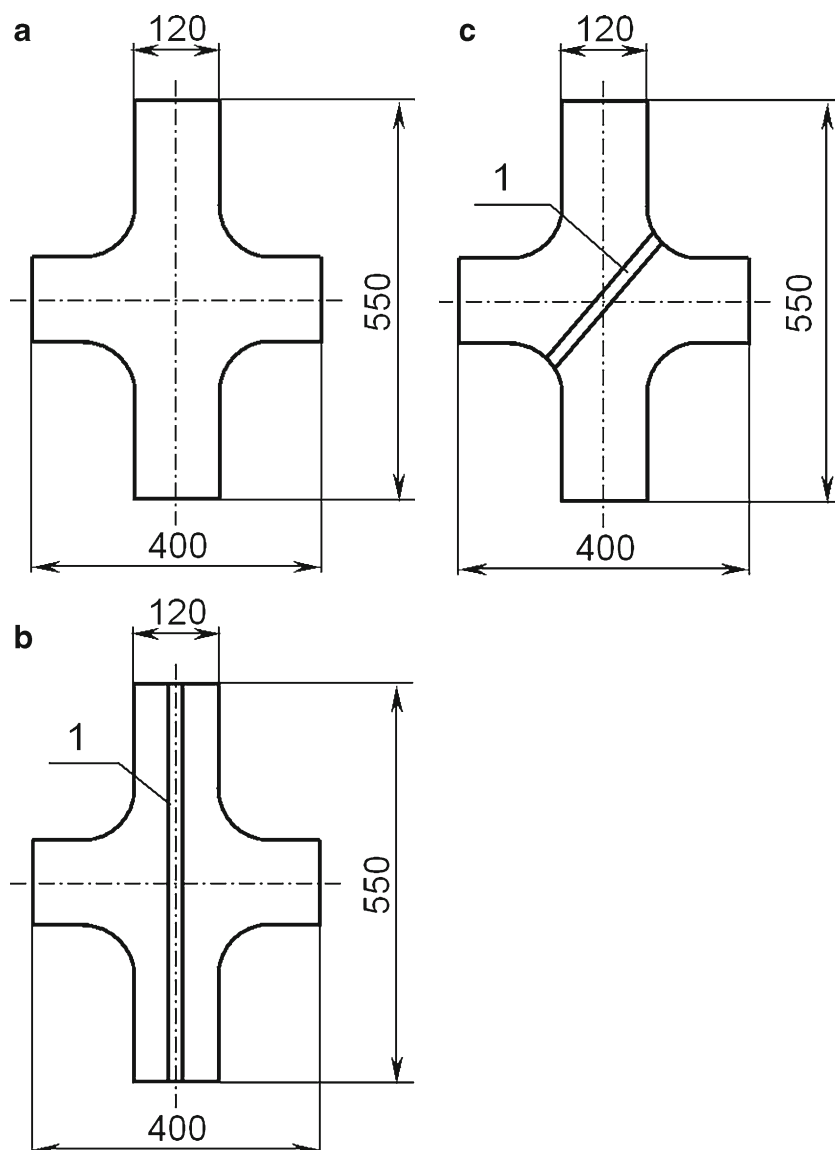
that at present lifetime assessment of metal components using the diagnostic parameters of the MMM method (variation of the magnetic field ΔH_L and its gradient $\Delta H_L/\Delta x$ in SCZs) is applied successfully in practice.

5 Testing of model (cruciform) specimens of base metal and welded joints of line pipes during cyclic load

To carry out quick assessment of steels' and welded joints' resistance to stress corrosion cracking (SCC) accelerated tests on standard specimens in corrosive medium are performed in various load conditions according to [9]. The main condition

for determination of metal's resistance to cracking based on comparison of failure time is precise determination of SCC cracks occurrence moment. Determination of this moment by indirect features (testing machine instruments' readings at the moment of load relief due to specimen strain) leads to occurrence of large measurement error. Besides, to confirm cracks formation it is required to terminate testing and specimen removal with subsequent visual examination.

The MMM method was applied during steel specimens testing under cyclic loading in the real-time mode in order to determine the moment of cracks occurrence. Testing of model (cruciform) specimens was carried out at Gubkin Oil & Gas University (Moscow).

Figure 14 shows basic dimensions of model specimens for testing of shell products ($\varnothing$1,420×21.5, steel of accuracy class X70 (17G2SAF)) in conditions of two-dimensional

Fig. 12 Variation of the tangential component intensity increase H_L^X of the SMLF in the point A of the specimen #4 of the type I depending of the number of tensile load cycles $(0.2 \div 0.95)\sigma_y$ at the frequency of 10 Hz

Fig. 14 Model specimens for SCC testing of shell products welded joint

stress state. Testing was carried out for the following model specimens:

- base metal specimen #70221 (see Fig. 14, *a*) with corrosion medium cell and without it (3 % water solution of NaCl)
- longitudinal weld specimen #70223 (see Fig. 14, *b*) with corrosion medium cell (3 % water solution of NaCl)
- spiral weld specimen #70224 (see Fig. 14, *c*) with corrosion medium cell (3 % water solution of NaCl)

Testing in conditions of two-dimensional stress state was carried out using the ZDM-100PU multipurpose pulsator machine. Figure 15 shows the locations of flux-gate transducers and the specimen on the testing machine.

A 16-channel sensor with flux-gate transducers allowing to record intensity of the normal and the tangential H_L field components was used during testing. Flux-gate transducers were installed opposite the central parts of the specimens in the assumed areas of fatigue cracks development.

It should be specially noted that the gap between the recording sensors and the specimen's surface allows, along with precise SMLF intensity measurement, to ensure mechanical stability of inspection plant, thus removing undesirable disturbances and damages due to
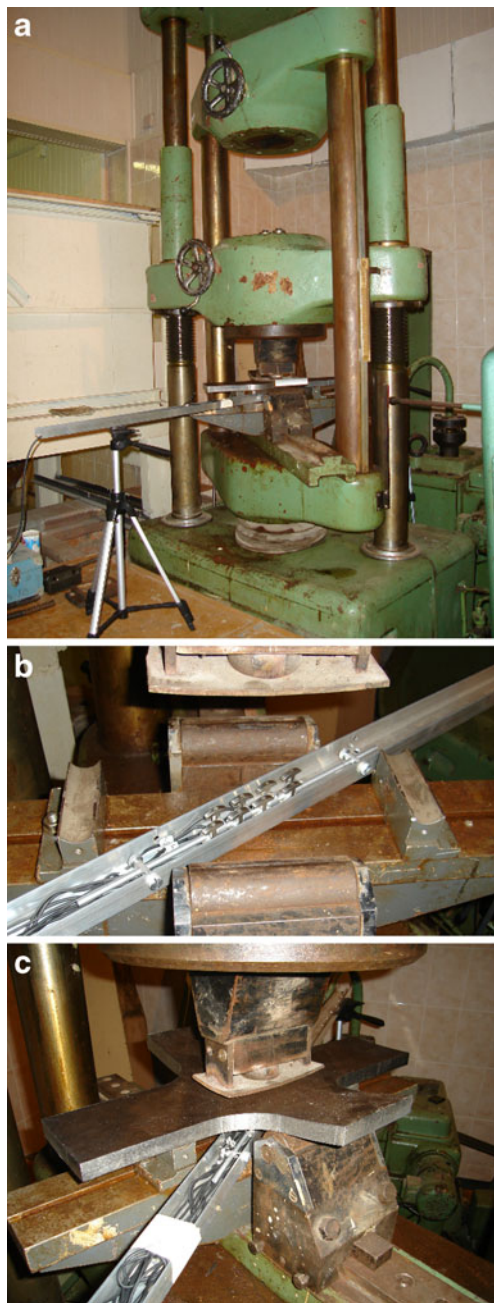
Fig. 15 ZDM-100 PU multipurpose pulsator machine and test device (**a**), locations of flux-gate transducers (**b**) and specimen (**c**) during testing

vibration loads occurring inevitably during contact inspection.

Figure 16 shows the pattern of model specimen loading and the location of loading device's elements. The 16-channel sensor data was recorded directly to the PC's

RAM using a special electronic unit. Figure 17 shows the typical magnetogram of the H_L field distribution recorded during the specimen testing by 16 measurement channels. The recording frequency of SMLF (H_L) intensity on each measurement channel was 187 Hz.

Bending load was applied in discrete steps to all specimens with increasing by 6 t every 200,000 cycles from the mark of 13 tons (13 t is a design load corresponding to stresses $0.9\sigma_{0.2}$ in the specimen's material in the upper support fixation area). Cycle asymmetry is $R = 0.8$. The bottom load limit is determined from the condition $P_{\min} = P_{\max} \times R$ for each stage of 200,000 cycles. The load application frequency is 500 cycles per minute (8.3 Hz).

As an example Table 3 shows the (air) test program for specimen #70221 (base metal). Figure 18 shows the magnetogram of the H_L field distribution recorded during testing of the specimen #70221. The total number of cycles up to failure (based on instruments readings and visible strain) for this specimen made 1,360,000 cycles.

To facilitate the data viewing Fig. 18 shows the H_L field graphs only for two measurement channels H_L-5 (H_L^X) and H_L-6 (H_L^Y), whose flux-gate transducers turned out to be located directly in the crack formation and opening area. H_L field variation in the course of cyclic load application was evaluated by the value of relative gradient $\Delta H_L / \Delta N$ depending on the number of load cycles.

Six segments with various patterns of the H_L field distribution are marked in Fig. 18. Segments I, III, and V are characterized by abrupt variations of the H_L field and of the relative gradient $\Delta H_L / \Delta N$. Segments II, IV, and VI are characterized by even H_p field distribution and of the relative gradient $\Delta H_L / \Delta N$ (which does not exceed $1 (A/m)/$ cycle and is comparable with the noise level). It should be noted that two abrupt variations of the H_L field, recorded on segment IV, was associated with load value variation.

While comparing segments I, III, and V with abrupt variations of the H_L field, it should be noted that their periodicity decreased as the number of load cycles grew. Segment V, on which на 7,000 load cycles took place, probably, corresponds to the fatigue crack opening period.

Figure 19 shows the magnetogram of the H_L field distribution on segment V during the period from 1,015,847 to 1,108,564 cycles (92,717 cycles in total). Area 3 of the magnetogram with abrupt change of H_L field distribution was marked for detailed review.

Figure 20 shows segment "I" with H_L field distribution of measurement channels H_L-5 (H_L^X) and H_L-6 (H_L^Y).
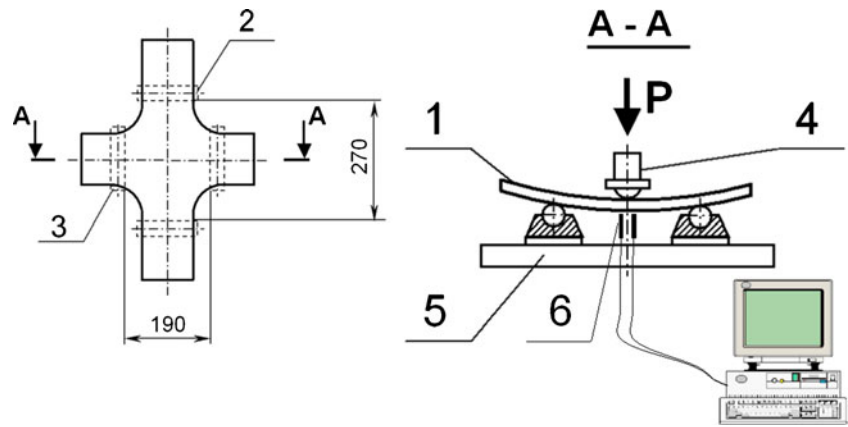
As an example, Fig. 21 shows scaled-up fragment of the area of abrupt distribution of the field intensity H_L (see Fig. 20) separately by measurement channels H_L-5 and H_L-6. The local field intensity variation area probably corresponding to the crack formation moment similar to those observed during testing of small-scale specimens (see Fig. 10). The pattern of H_L field's intensity variation corresponded to that early revealed during testing of steel specimens in conditions of uniaxial cyclic loading at the moment of explosion. Similar results were obtained during testing of specimens #70223 and #70224.

6 Analysis of the results and conclusions

1. The obtained results of specimens investigation confirmed experimentally the earlier drawn conclusion about the possibility of application of the MMM method and of the appropriate inspection instruments for quick testing of mechanical properties and cyclic strength parameters at the physical level.

2. Comparison of strain diagrams $\sigma{-}\varepsilon$ and magnetograms $\sigma{-}H_L^X$, $H_L^X{-}\varepsilon$, obtained in the mode of static loading (see Figs. 3, 4, 5, and 6), of the diagrams of cyclic loading $\sigma{-}\varepsilon$ (see Fig. 10) and corresponding magnetograms (see Figs. 7, 8, and 9) confirms once more the earlier established correlation of magnetomechanical parameters, conditioned by the "magnetodislocation hysteresis".

3. In the process of cyclic loading, a linear dependence was established between the amplitude of resistance to straining $\Delta\varepsilon$ and the variation amplitude of the self-magnetic field ΔH of the metal of the specimen.

Fig. 17 Typical magnetogram of the H_L field variation recorded during the specimen testing by 16 measurement channels
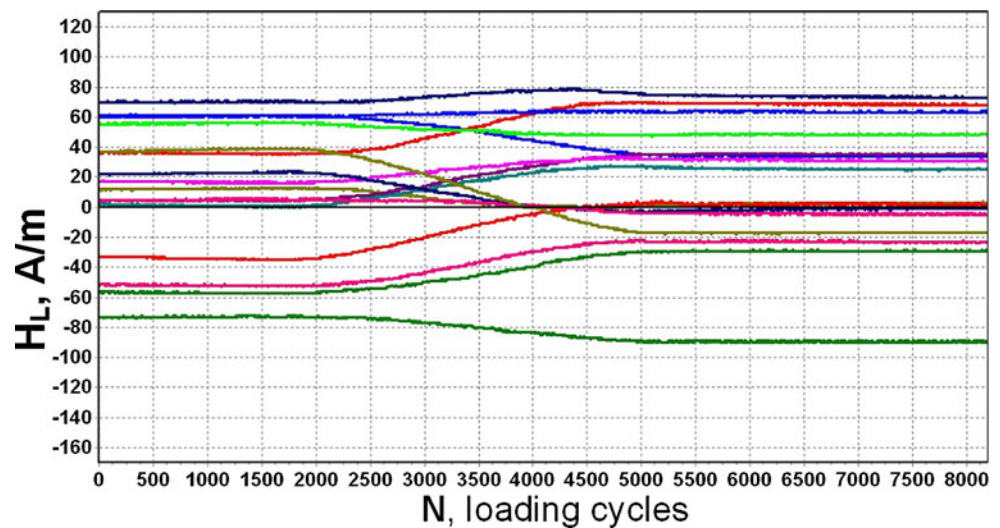
Table 3 Test program for specimen #70221

Load (tons)	Loading period
13	0÷200,000 cycles
18	200,000÷400,000 cycles
24	400,000÷600,000 cycles
30	600,000÷800,000 cycles
36	800,000÷1,000,000 cycles
42	1,000,000÷1,360,000 cycles

4. The effect of abrupt decline and instantaneous growth of resistance to straining was recorded for the first time at the maximum of the applied tensile load of each cycle using the parameters of the magnetic memory of metal. The aforementioned effect was not observed at the minimum of the amplitude of the cyclic tensile load. The display of the effect of short-time variation of resistance to straining at the maximum of the cyclic tensile load increases gradually as the number of cycles grows and meets the maximum value by the amplitude between the decline and growth of resistance to straining directly before failure of the specimen. Based on the earlier conducted experimental investigations [2], it can be assumed that the revealed

effect characterizes growth of metal damaging in the form of accumulation and gradual increasing of dislocations density in a SCZ, being the site of potential failure of the specimen.

5. The fatigue curves, plotted by variation of the self-magnetic field of the specimens in the course of cyclic loading, confirm experimentally the possibility of lifetime assessment of metal components by the parameters of the magnetic memory of metal.

6. The magnetograms, recorded during cyclic loading of specimens in the real-time mode, allow declaring the possibility to use the MMM method and the TSC-type instruments for monitoring of the technical state directly during operation of the pressure equipment. Taking into account that various types of noise do not influence the diagnostic parameters of the MMM method and that no special additional loading is required, the TSC-type instruments and the appropriate sensors (which do not require the direct contact with the inspection object) have obvious advantage over the AE instruments, which are widely used in practice for monitoring of the technical state of metal components.

7. During testing of model cruciform specimens gradual growth of average H_p field value was observed
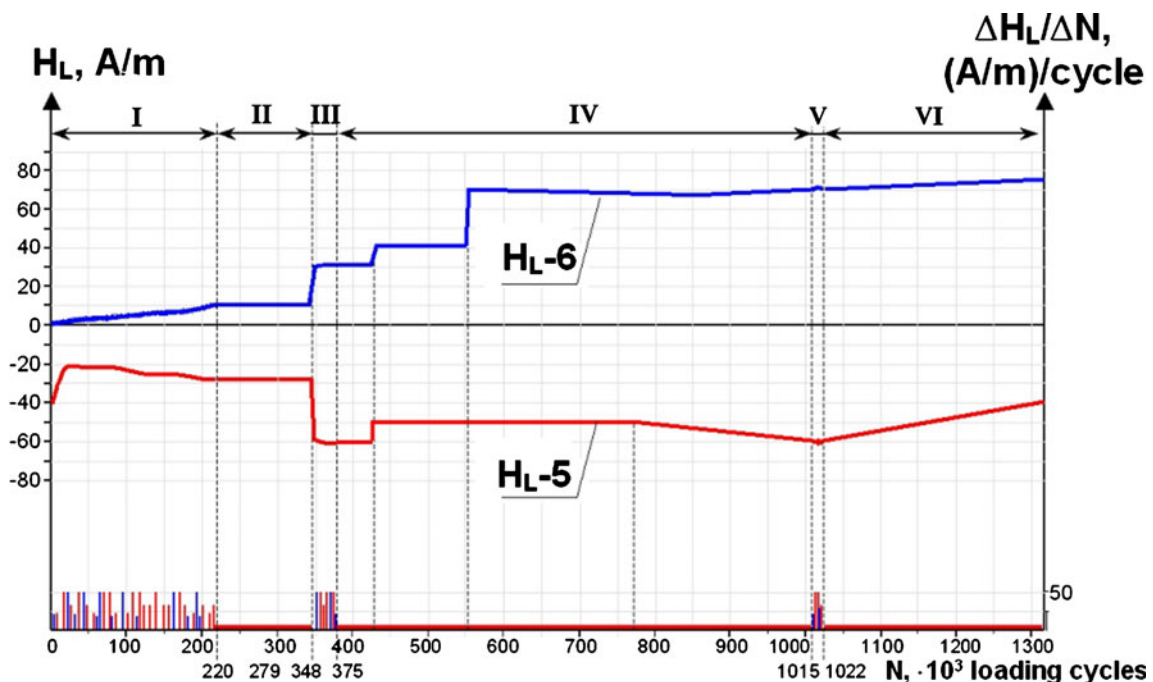
Fig. 18 Magnetogram of the H_L field distribution recorded during testing of the specimen #70221
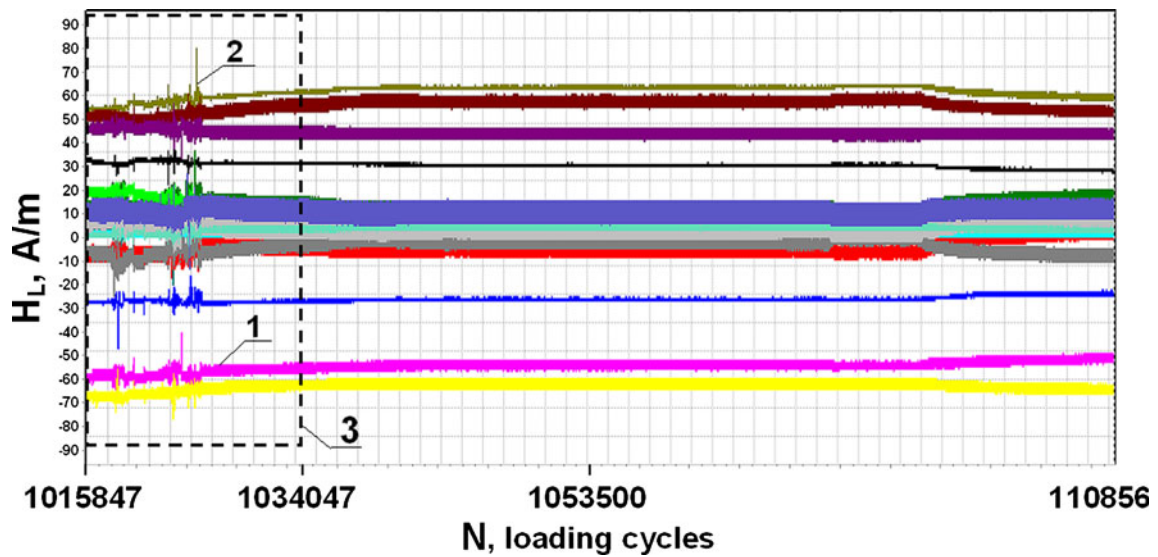
Fig. 19 Magnetogram with H_L field distribution during the period from 1,007,000 to 1,100,000 (1,015,847÷1,108,564) cycles (about 93,000 cycles) by all measurement channel: *1* channel H_L-5 for measurement of the tangential field component H_L^X; *2* channel H_L-6 for measurement of the normal field component H_L^Y; *3* area of abrupt change of the field intensity H_L distribution

on average by 40 A/m compared to the initial value as well as of oscillation amplitude from 1–2 to 8–10 A/m.

8. The signal from the probable crack propagation beginning was registered in conditions of two-dimensional stress state by using the MMM method 300,000 cycles before the visible failure of the

cruciform specimen #70221 made of pipeline shell base metal.

9. It should be noted that testing of the specimen #70221 was carried out with forced stop for periodic shutdown of the testing machine. It is recommended in future to perform similar testing without the plant shutdown in order to remove the stress relaxation and metal hardening effect.
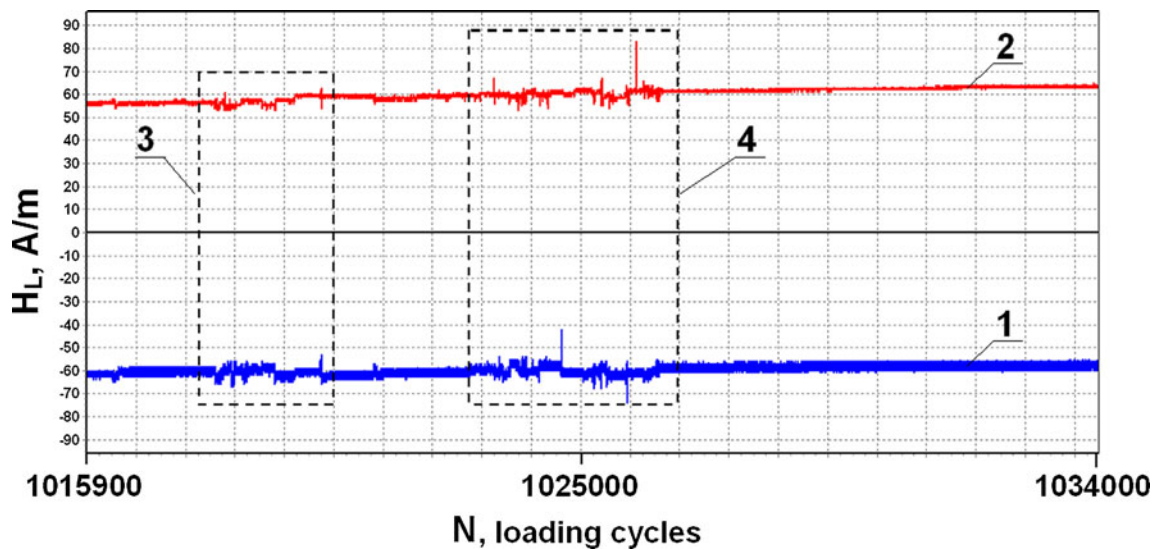

Fig. 20 Segment V on the magnetogram of H_L field distribution during the period from 1,015,900 to 1,034,000 cycles: *1* channel H5 for measurement of the field intensity tangential component H_L^X; *2* channel H6 for measurement of the field intensity normal component H_L^Y; *3* the first observed segment of abrupt H_L field variation; *4* the second observed segment of abrupt H_L field variation

Fig. 21 H_L field distribution separately by measurement channels H_L-5 and H_L-6 in local areas of intensity variation: *1* channel H_L-5 for measurement of the field intensity tangential component H_L^X; *2* approximating curve of distribution of the field intensity tangential component H_L^X of channel H_L-5; *3* channel H_L-6 for measurement of the field intensity normal component H_L^Y; *4* approximating curve of distribution of the field intensity normal H_L^Y of channel H_L-6
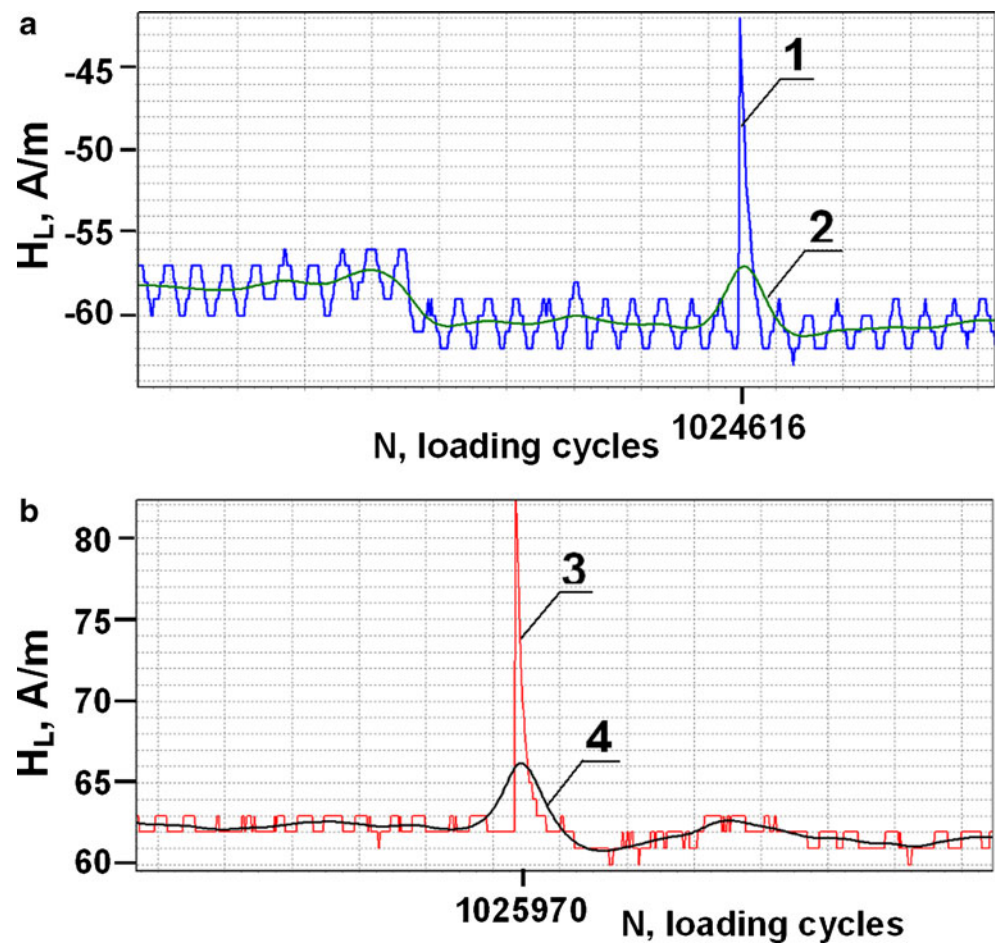
References

1. Vlasov VT, Dubov AA (2004) Physical bases of the metal magnetic memory method. ZAO "TISSO", Moscow, p 424
2. IIW document **V-1347-06** Training handbook. The method of metal magnetic memory (MMM) and inspection instruments
3. ISO 24497–1 (2007) (E) Non-destructive testing—metal magnetic memory—Part 1: Vocabulary
4. ISO 24497–2 (2007) (E) Non-destructive testing—metal magnetic memory—Part 2: General requirements
5. ISO 24497–3 (2007) (E) Non-destructive testing—metal magnetic memory—Part 3: Inspection of welded joints
6. Dubov AA (1997) Investigation of metal properties using the effect of the magnetic memory of metal//Physical metallurgy and heat treatment of metals, 9
7. Goritsky VM, Dubov AA, Demin EA (2000) Investigation of structural damageability of steel samples using the metal magnetic memory method. Control Diagnostics 7:35–39
8. Makhutov N.A., Dubov A.A., Kolokolnikov S.M., Denisov A.S. (2008) Investigation of steel specimens for static and cyclic load using the metal magnetic memory method. Proceeding of 21st International Congress and Exhibition COMADEM-2008 (Condition Monitoring and Diagnostic Engineering Management), Czech Republic, Prague, June 11–13. p. 319–330
9. Standard of JSC "GAZPROM" 2–5.1-148-2007. Testing methods of steel and welded joints stress corrosion cracking